

Milli-Hertz Gravitational Wave Background Produced by Quasi-Periodic Eruptions

XIAN CHEN,^{1,2} YU QIU,¹ SHUO LI,³ AND F. K. LIU^{1,2}

¹*Astronomy Department, School of Physics, Peking University, Beijing 100871, China*

²*Kawli Institute for Astronomy and Astrophysics, Peking University, Beijing 100871, China*

³*National Astronomical Observatories, Chinese Academy of Sciences, Beijing 100012, China*

Abstract

Extreme-mass-ratio inspirals (EMRIs) are important targets for future space-borne gravitational-wave (GW) detectors, such as the Laser Interferometer Space Antenna (LISA). Recent works suggest that EMRI may reside in a population of newly discovered X-ray transients called “quasi-periodic eruptions” (QPEs). Here we follow this scenario and investigate the detectability of the five recently discovered QPEs by LISA. We consider two specific models in which the QPEs are made of either stellar-mass objects moving on circular orbits around massive black holes (MBHs) or white dwarfs (WDs) on eccentric orbits around MBHs. We find that in either case each QPE is too weak to be resolvable by LISA. However, if QPEs are made of eccentric WD-MBH binaries, they radiate GWs in a wide range of frequencies. The broad spectra overlap to form a background which, between 0.003 – 0.02 Hz, exceeds the background known to exist due to other types of sources. Presence of this GW background in the LISA band could impact the future search for the seed black holes at high redshift as well as the stellar-mass binary black holes in the local universe.

Keywords: Gravitational waves (678) — Intermediate-mass black holes (816) — White dwarf stars (1799) — X-ray transient sources (1852)

1. INTRODUCTION

An extreme-mass-ratio inspiral (EMRI) consists of a massive black hole (MBH) and a small compact object, such as a stellar-mass black hole (BH), a neutron star, or a white dwarf (WD), moving on a tightly bound orbit (Amaro-Seoane et al. 2007). Because of gravitational-wave (GW) radiation, the orbit decays and the small object eventually coalesces with the MBH. If the mass of the MBH is $10^5 - 10^7 M_\odot$, the GW radiated during the last few years of the system falls in the sensitive band of the Laser Interferometer Space Antenna (LISA, Amaro-Seoane et al. 2017). During this period, as many as $10^4 - 10^5$ GW cycles could be accumulated in the data stream, providing rich information about the spacetime geometry close to a MBH (Gair et al. 2013; Berry et al. 2019).

Despite their scientific importance, many basic properties of EMRIs, such as the event rate, are largely unconstrained. The difficulty lies in the lack of a distinctive electromagnetic (EM) signature. For example,

the EMRIs containing stellar-mass BHs are considered to dominate the EMRI population (de Freitas Pacheco et al. 2006), but the predicted event rate varies from one dozen per year (within a redshift of $z = 4.5$) to as high as a few $\times 10^4$ per year (see Babak et al. 2017; Gair et al. 2017, for a summaries). The redshift distribution is also uncertain. If most EMRIs are at high redshift, they would form a GW background which is practically indistinguishable from noise (Sigl et al. 2007; Bonetti & Sesana 2020).

Unlike stellar-mass BH or neutron star, a WD revolving around a MBH could be tidally detonated if the MBH has moderate mass ($10^3 - 10^6 M_\odot$, e.g. Luminet & Pichon 1989; Rosswog et al. 2009), or it could activate the MBH via Roche-lobe overflow and tidal disruption (e.g. Ivanov & Papaloizou 2007; Zalamea et al. 2010; MacLeod et al. 2014). Therefore, the EMRIs containing WDs are potential targets for joint EM and GW observations (Sesana et al. 2008). In particular, they encode valuable information about the astrophysical environments which lead to the formation of EMRIs. In theory, various dynamical processes could deliver WDs to the vicinity of MBHs, including dynamical relaxation of star cluster (Hills & Bender 1995), tidal capture (Ivanov

& Papaloizou 2007), partial disruption of red giant stars (Bogdanović et al. 2014), and tidal separation of WD binaries (Miller et al. 2005). It is estimated that as many as 10^2 such EMRIs could be detected by LISA with reasonable signal-to-noise ratio (SNR, Hills & Bender 1995; Sigurdsson & Rees 1997; Ivanov 2002; Sesana et al. 2008).

Interestingly, the EM counterpart to the above WD EMRI may have been found in a new type of transient called “quasi-period eruption” (QPE, Miniutti et al. 2019; Giustini et al. 2020; Arcodia et al. 2021; Chakraborty et al. 2021). Five QPEs have been discovered so far and they share a distinctive feature: within an hour the X-ray count rate surges by one to two orders of magnitude and such an eruption recurs every few hours. The short duration of each outburst and the short recurrence timescale resemble the characteristics of a small object swooping by a MBH periodically along a tightly bound, highly eccentric orbit. The similarity leads to the suggestion that QPEs are powered by eccentric WD EMRIs whose WDs are filling up their Roche lobes and feeding the MBHs during their pericenter passages (King 2020; Zhao et al. 2021). This interpretation is further supported by the observational evidence of earlier tidal disruption events in two of the QPEs (Miniutti et al. 2019; Sheng et al. 2021; Chakraborty et al. 2021), corroborating the picture that partial disruption of stars could deposit their compact cores (such as WDs) to the close vicinity of MBHs.

Further theoretical studies suggest that WD-MBH binaries may be too short-lived to explain the detection rate of QPEs because the WDs would expand in a runaway fashion as soon as the mass transfer starts (Metzger et al. 2021). One way of alleviating the problem invokes less eccentric orbits for those objects (not necessarily WDs) around MBHs, so that mass transfer can be avoided (Metzger et al. 2021; Xian et al. 2021; Ingram et al. 2021). In these models, QPEs also emit GWs because they are essentially still EMRIs. Another class of models do not rely on EMRIs but attribute the X-ray eruption to the instability of accretion disk (Miniutti et al. 2019; Motta et al. 2020; Sniegowska et al. 2020; Raj & Nixon 2021). In this case, little GW radiation is expected. These models, however, have difficulties explaining two of the QPEs which are found in quiescent galaxies showing no sign of accretion disks (Arcodia et al. 2021).

Although QPEs may contain EMRIs, whether they can be detected by LISA is still unclear. The conventional way of evaluating the detectability of a GW source by its characteristic strain (see, e.g., Sesana et al. 2008; Zhao et al. 2021, for WD EMRIs) could be insufficient

for QPEs. First, the characteristic strain is useful, i.e., it is positively correlated with the SNR, only if the GW frequency increases rapidly during the observational period. Such a signal is called “chirp signal” (e.g. Robson et al. 2019). This is not the case for QPEs because, if they are EMRIs, their orbits evolve on a timescale of $10^3 - 10^4$ years according to the previous studies (e.g. King 2020; Metzger et al. 2021; Ingram et al. 2021). Such a timescale is much longer than the mission duration of LISA. As a result, the SNR is suppressed substantially. Second, when the orbital eccentricity is high, as would be the case if QPEs are powered by WDs (e.g. King 2020), the GW power is emitted in a wide range of harmonic frequencies (Peters & Mathews 1963). Only those harmonics falling in the sensitive band of LISA contribute to the SNR. Third, recent study of the EMRIs with stellar BHs suggests that although the majority are unresolvable by LISA, together they form a background which may be higher than the instrument noise (Bonetti & Sesana 2020). Whether QPEs produce a similar background deserves investigation. Understanding this background is important because it may impinge on the detection of the seed MBHs at high redshift, as well as the binary BHs (BBHs) which could be the progenitors of the sources already detected by the Laser Interferometer Gravitational-wave Observatory (LIGO) and the Virgo detectors (e.g. Bonetti & Sesana 2020).

Here we take the above three factors into account and study the detectability of QPEs by the future LISA mission. The paper is organized as follows. In Section 2, we describe two models proposed for QPEs which contain EMRIs. Based on these models, we calculate the corresponding GW spectra for the five detected QPEs. In Section 3 we compute the GW background formed by QPEs and investigate its detectability by LISA. We also compare it with the GW background due to other types of sources and evaluate the impact on the future search of seed BHs and BBHs by LISA. In Section 4 summarize our results and discuss the caveats. Throughout the paper, we assume a standard Λ CDM cosmology with the parameters $H_0 = 70 \text{ km s}^{-1} \text{ Mpc}^{-1}$, $\Omega_\Lambda = 0.7$, and $\Omega_M = 0.3$.

2. MODELS

2.1. EMRIs on circular orbits

We first consider a model in which QPEs are produced by stellar-mass objects moving on relatively circular orbits around MBHs (Metzger et al. 2021; Xian et al. 2021). Such an orbit has three parameters, the mass of the MBH M , the mass of the stellar-mass object m , and the orbital period P . For the five QPEs detected so far,

we give their parameters in Table 1 which are derived in the following ways.

The orbital period P is determined by the time interval between successive eruptions. Note that in some models, the small object collides with the accretion disk of the MBH twice per orbital period, and hence P is twice the time interval between eruptions (Xian et al. 2021). We neglect this factor of two because it does not qualitatively affect the amplitude and detectability of the GWs.

The mass M of the MBH is not an observable and is derived for different QPEs using different methods. For GSN 069 and RX J1301.9+2747, the masses are derived from fitting their X-ray spectra with accretion disk models (adopted from Miniutti et al. 2019; Shu et al. 2017). The mass of XMMSL1 J0249-041244 is inferred from the correlation between the mass of a MBH and the velocity dispersion of the bulge of the host galaxy (from Wevers et al. 2019). For eRO-QPE1 and eRO-QPE2, since the masses of their host galaxies have been derived in previous works (Arcodia et al. 2021), we use them to estimate the masses of the MBHs according to the empirical scaling relation

$$\log(M_{\text{BH}}/M_{\odot}) = 7.45 + 1.05 \log(M_{\text{stellar}}/10^{11}M_{\odot}) \quad (1)$$

(Reines & Volonteri 2015).

The mass m of the small object is model-dependent and uncertain. To accommodate various theoretical possibilities, we treat m as a free parameter and vary it between $0.2M_{\odot}$, mimicing WDs or stripped cores of main-sequence stars, to $10M_{\odot}$, accounting for massive main-sequence stars or stellar-mass BHs.

Given the above parameters and assume that the orbits are circular, the GW radiation timescale (Peters 1964) is many orders of magnitude longer than the mission duration of LISA, about $t_{\text{LISA}} = 4$ years. In this case, the GW spectrum is essentially monochromatic and the increment of frequency Δf during the observational period is much smaller than the GW frequency f . Note that for circular orbits $f = 2/P$.

In this situation, the SNR can be calculated with

$$\text{SNR}^2 = \frac{h_c^2 \Delta f}{f^2 S(f)}, \quad (2)$$

where h_c is the characteristic strain and $S(f)$ is the one-side amplitude spectral density of LISA (Robson et al. 2019). According to the last equation, the effective strain, which is directly proportional to the SNR, is

$$h_{\text{eff}} = h_c \sqrt{\Delta f / f} \quad (3)$$

(also see Barack & Cutler 2004). It is smaller than the normally adopted characteristic strain h_c of a fast chirp signal by a factor of $\sqrt{\Delta f / f}$.

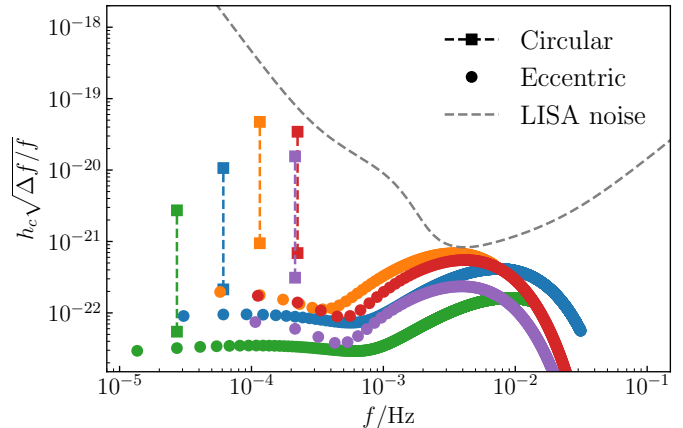


Figure 1. The effective GW strain of QPEs (colored squares and solid dots) versus the LISA sensitivity curve $\sqrt{fS(f)}$ (grey dashed line). The squares connected by dashed lines correspond to the model in which QPEs contain circular binaries. The dots refer to the model in which QPEs are powered by WDs on eccentric orbits around MBHs.

The effective strain computed using the above model and assuming $t_{\text{LISA}} = 4$ years is shown in Figure 1 as the squares connected by dashed lines. Each QPE is represented by a vertical line segment because we have allowed m to vary between 0.2 and $10M_{\odot}$. They are all below the LISA sensitivity curve $\sqrt{fS(f)}$, suggesting that LISA could not detect such QPEs.

2.2. WDs on eccentric orbits

We now consider another model in which the small object in a QPE is a WD and it is moving along a highly eccentric orbit around the central MBH (King 2020). In this model, GW radiation causes the orbital pericenter to decay until the WD fills the Roche lobe and starts feeding the MBH. Such a system can be characterized by four parameters: besides M of the MBH and m of the WD, there are also the semimajor axis a and eccentricity e of the orbit. Following King (2020), we derive these parameters using their relationships with the observables of QPEs. The basic steps are given below.

We first adopt the MBH mass M and orbital period P from the previous subsection. Then the semimajor axis can be derived from $P = 2\pi(GM/a^3)^{-1/2}$. To establish a relationship between the remaining two parameters, m and e , we use the physical requirement that the mass-transfer timescale m/\dot{M} equals the decay timescale of the pericenter $|r_p/\dot{r}_p|$, where \dot{M} is the orbit-averaged accretion rate of the MBH and $r_p = a(1-e)$ is the pericenter distance. Throughout this paper, the dot symbol denotes the time derivative.

The accretion rate \dot{M} is determined by the light curve of the eruptions. From the peak luminosity L of an

Table 1. QPE sample and their parameters

Source	z	M/M_\odot	P/ks	$\Delta t/\text{ks}$	$L/\text{erg s}^{-1}$	m/M_\odot	e	Ref.
GSN 069	0.018	4.0×10^5	31.55	2.05	5.0×10^{42}	0.322	0.972	Miniutti et al. (2019)
RX J1301.9+2747	0.02358	1.8×10^6	16.5	1.2	1.4×10^{42}	0.150	0.928	Giustini et al. (2020)
eRO-QPE1	0.0505	9.1×10^5	66.6	13.7	3.3×10^{42}	0.461	0.986	Arcodia et al. (2021)
eRO-QPE2	0.0175	2.3×10^5	8.64	0.8	1.0×10^{42}	0.178	0.901	Arcodia et al. (2021)
XMMSL1 J024916.6-041244	0.019	8.5×10^4	9	1	3.4×10^{41}	0.169	0.901	Chakraborty et al. (2021)

eruption and its full width at half-maximum Δt , we get $\dot{M} = L\Delta t/(\eta Pc^2)$, where η is the radiative efficiency and c is the speed of light. To write $|r_p/\dot{r}_p|$ in terms of a and e , we note that the specific angular momentum $J = \sqrt{G(M+m)a(1-e^2)}$ is proportional to $\sqrt{r_p}$ when $e \simeq 1$. Therefore, we can write $m/\dot{M} \simeq |J/\dot{J}|$. We note that according to Peters (1964), $|J/\dot{J}|$ is proportional to $(1-e^2)^{5/2}$, not $(1-e^2)^{7/2}$ which is related to the loss of orbital energy and has been misused in the previous works (e.g. King 2020; Zhao et al. 2021).

To close the equations we need another relationship between m and e . This is given by the condition of Roche-lobe overflow. It requires that during the pericenter passage the WD, which has a size of about $0.013R_\odot(m/M_\odot)^{-1/3}$, fills the Roche lobe, whose radius is $0.46r_p(m/M)^{1/3}$ (King 2020). Finally, we find that

$$m \simeq 0.20C^{-15/22}M_\odot, \quad (4)$$

$$e \simeq 1 - 0.072C^{5/11}P_4^{-2/3}, \quad (5)$$

where

$$C = \left(\frac{M}{10^5 M_\odot}\right)^{4/15} \left(\frac{L \Delta t}{10^{45} \text{erg}}\right)^{-2/5} \left(\frac{\eta}{0.1}\right)^{2/5} \quad (6)$$

and $P_4 = P/(10^4 \text{s})$.

The values of the observables, Δt and L , as well as the derived physical parameters, m and e , are given in Table 1. We find that m falls in the typical mass range of WDs, suggesting that the model is self-consistent. Moreover, e is higher than 0.9, consistent with the scenario that the WDs are delivered to the MBHs by either partial tidal disruption or binary separation, though the event rate is expected to be low (Metzger et al. 2021).

Because the binary is now eccentric, the GW radiation is spread into a wide range of harmonic frequencies (Peters & Mathews 1963). We use the formulae derived in Barack & Cutler (2004) to compute the characteristic strain $h_{c,n}$ of the n th harmonic, which is at the frequency n/P . The effective strain, which is directly correlated with the SNR, is computed with $h_{c,n}\sqrt{\Delta f/f}$ (Barack & Cutler 2004) and shown in Figure 1 as the colored dots.

It is clear that each QPE is now emitting a wide GW spectrum. We find that the peak of the spectrum occurs

at a frequency of about $\sqrt{GM/r_p^3}$, which can be understood due to the fact that the strongest GW radiation is produced when the WD passes the orbital pericenter. We also find that the frequency of the peak coincides with the most sensitive band of LISA, around 3 millihertz (mHz). However, the effective strain remains below the sensitivity curve of LISA, indicating that LISA cannot detect an individual QPE with sufficient SNR.

3. GW BACKGROUND

Although an individual QPE is too weak to detect by LISA, several QPEs together may increase the SNR. This could happen if QPEs are made of WDs on eccentric orbits around MBHs. In this case, the GW spectrum is broad, as we have seen in the previous section. The broadness increases the chance of signal overlapping at the same frequency. For this reason, we use the model described in Section 2.2 to estimate the combined GW signal of many QPEs.

First, we determine how many QPEs exist per unit comoving volume. Based on the five QPEs detected so far (Table 1), we infer a comoving number density of $n_* \simeq 120 \text{Gpc}^{-3}$. We use this value for the later calculation of the GW background. However, we caution that it should be regarded as a lower limit for two reasons. (i) The current QPE sample is by no means complete because it is compiled from heterogeneous observations. (ii) Many more WD-MBH binaries are expected to reside on wider orbits because the evolution timescale (GW radiation timescale) is longer for wider binaries. Wide binaries also emit GWs but not necessary X-rays because the mass transfer may not have started. Therefore, they are not included in the QPE sample.

Second, assuming that the comoving number density n does not evolve with redshift, we generate a mock sample of 18,000 QPEs in the redshift range of $0 \leq z \leq 1$. We do not consider higher redshift mainly because our result converges as z approaches 1, as we will see later. For each mock QPE, we randomly choose one of the five detected QPEs in Table 1 and assign the parameters M, m, P, e of the selected QPE to the mock one. Having specified the parameters, we then compute the effective

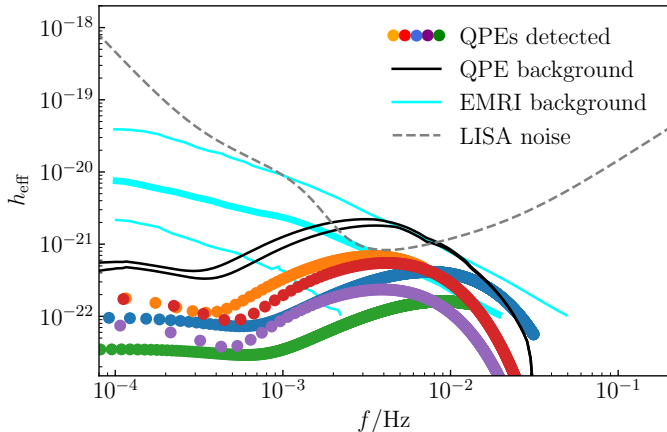


Figure 2. The minimum GW background produced by QPEs (black solid curves). There are two black curves because they refer to the contribution from the QPEs at, respectively, $z \leq 0.5$ and $z \leq 1$. The effective strain of the five detected QPEs are also shown (colored dots) for comparison. The three cyan curves show the background produced by the EMRIs containing stellar-mass BHs, and from top to bottom they refer to the most optimistic, fiducial, and the most pessimistic estimations (from Bonetti & Sesana 2020).

strain as is seen by LISA (following Barack & Cutler 2004). In the calculation, we assume $t_{\text{LISA}} = 4$ years.

Third, the GW signals of different QPEs add up incoherently, so the total effective strain h_{eff} is computed with

$$h_{\text{eff}}^2(f) = \sum_i h_{\text{eff},i}^2(f), \quad (7)$$

where $h_{\text{eff},i}$ denotes the effective strain of the i th QPE of our mock sample. The result is shown in Figure 2 as the two black solid curves, which refer to the background produced by the QPEs at, respectively, $z \leq 0.5$ and $z \leq 1$. The corresponding SNR is 2.1 and 2.5, where we have calculated the total SNR of the GW background with

$$\text{SNR}^2 = \int \frac{h_{\text{eff}}^2(f)}{fS(f)} d \ln f. \quad (8)$$

We emphasize that the QPE background derived here should be regarded as a lower limit because it is computed based on the most conservative estimation of the number density of QPEs, i.e., only five QPEs within a redshift of 0.05. Nevertheless, we find that in the frequency band of 4 – 20 mHz the QPE background is comparable to the most optimistic estimation of the GW background produced by those EMRIs containing stellar-mass BHs (see the highest cyan curve in Fig. 2). The QPE background is also orders of magnitude higher than the GW background generated by tidal disruption events (see Toscani et al. 2020, not shown here). There-

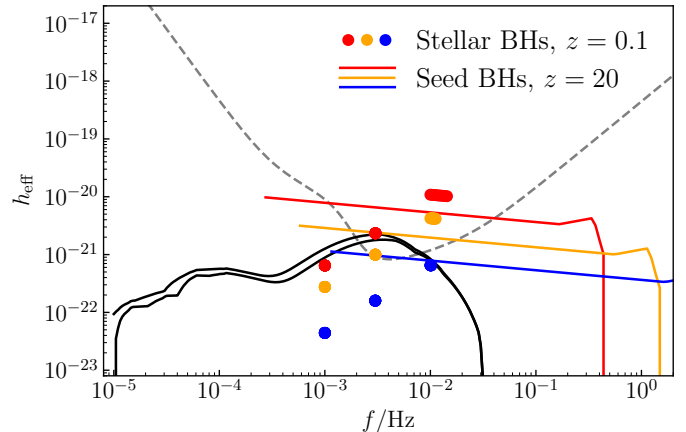


Figure 3. Comparing the GW background produced by QPEs (black solid curves) with other GW sources. The colored curves represent the chirping signals of merging seed BHs at redshift $z = 20$. From top to bottom, the red, orange, and blue curves correspond to a chirp mass of, respectively, 1000, 300, and $100 M_{\odot}$. The colored dots show the effective strain of inspiraling stellar-mass BHs residing at three representative frequencies (1, 3, 10) mHz and a redshift of $z = 0.1$. The red, orange, and blue dots correspond to a chirp mass of 50, 30, and $10 M_{\odot}$. An observational period of $t_{\text{LISA}} = 4$ years is assumed in the calculation.

fore, we conclude that QPE is an important source of stochastic GW background in the mHz band, in fact the most sensitive band of LISA.

Bonetti & Sesana (2020) pointed out that an excessive GW background in the mHz GW band would impinge on several science goals of LISA, including the search for seed MBHs at $z \gtrsim 20$ as well as detecting stellar-mass BBHs in their early inspiral phase. To understand the ramification of our results, we show in Figure 3 the GW signals of seed MBHs and stellar-mass BBHs and compare them with the background due to QPEs. We find that the QPE background is higher than the chirp signal of a MBH binary at $z = 20$, if the chirp mass is lower than $300 M_{\odot}$. Such a mass corresponds to the seed BHs produced by population-III stars (Volonteri 2010). We also find that at $f \lesssim 3$ mHz the QPE background becomes higher than the effective strain of a stellar-mass BBH at $z = 0.1$, if the chirp mass is smaller than $50 M_{\odot}$. The progenitors of many LIGO/Virgo BBHs fall in this mass range. These results highlight the necessity of observationally compiling a complete sample of QPEs to put a better constraint on the level of the GW background.

4. SUMMARY AND DISCUSSION

Motivated by the suggestion that the recently discovered QPEs may contain EMRIs, we have calculated in

this paper the GW spectra and studied their detectability by LISA. We investigated two scenarios proposed in the literature, in which the orbits of the EMRIs are, respectively, circular and highly eccentric ($e > 0.9$). We found that in both cases the signal of an individual QPE is too weak to be discernible by LISA (Fig. 1).

This conclusion differs from the one made by Zhao et al. (2021), mainly because we noticed that the systems are evolving on a timescale much longer than the mission duration of LISA, so that the number of GW cycles accumulated in the LISA band is greatly suppressed relative to the number of cycles coming from fast-chirping sources. Sesana et al. (2008); Han & Fan (2018) also studied the GW signal of a WD around an intermediate-massive BH (IMBH). We notice that the SNR derived by them is much higher than the detection threshold of LISA. This result is caused by the fact that their WDs are only a few years away from the final merger with the IMBHs, while our QPEs are thousands of years before the merger. The GW radiation is much weaker in our case.

More importantly, we found that if the EMRIs in QPEs are eccentric, their broad GW spectra could overlap in a wide range of frequencies, producing a background which has a much higher SNR. We showed that this background is already higher than the LISA noise curve even if we adopt the most conservative assumption about the abundance of QPEs (Fig. 2). Moreover, in the frequency band of 4–20 mHz, the QPE minimum background is comparable to the most optimistic estimation of the background from the fiducial EMRIs, i.e., those EMRIs containing stellar-mass BHs. This result implies that QPE may be the dominant source of confusion noise in the most sensitive band of LISA. We have shown that its presence may affect the future search for seed BHs and stellar-mass BBHs by LISA (Fig. 3).

When calculating the GW background, we mentioned that our model missed the WD-MBH binaries on wide orbits (because they have not started mass transfer and will not be detected as QPEs). We can roughly estimate the contribution of these binaries to the SNR of the GW background. Suppose that within the orbital period of P to $P + dP$ there are a number of dN WD-MBH bi-

aries. The number density, dN/dP , is proportional to $1/|\dot{P}|$ according to the continuity equation. This relation leads to $dN/d\ln P \propto |P/\dot{P}|$. In our problem, \dot{P} is determined by GW radiation, and during the evolution of P , the pericenter distance r_p is more or less conserved, due to the fact that $|P/\dot{P}|/|r_p/\dot{r}_p| \sim (1-e) \ll 1$. In this case, we can derive $dN/d\ln P \propto r_p^{7/2} P^{1/3}$, where we have used the relation $P/\dot{P} \propto a/\dot{a} \propto a^4(1-e)^{7/2}$ (Peters 1964). If we can further estimate the effective strain h_{eff} of such a WD-MBH binary, we can derive the SNR contributed by these $dN/d\ln P$ binaries as $d(\text{SNR}^2)/d\ln P \sim h_{\text{eff}}^2(dN/d\ln P)$. For h_{eff} , we have seen that it peaks at a frequency of $f_p \sim (GM/r_p^3)^{1/2}$, due to the fact that most of the GW energy is radiated during the pericenter passage. Therefore, the corresponding effective strain can be calculated with $h_{\text{eff}}^2 \propto (\dot{E}_{\text{tot}}/\dot{f}_p)(\dot{f}_p/f_p)t_{\text{LISA}}$, where \dot{E}_{tot} is the total power of GW radiation (Barack & Cutler 2004). Finally, we find that $h_{\text{eff}}^2 \propto P^{-1}r_p^{-2}t_{\text{LISA}}$, and $d(\text{SNR}^2)/d\ln P \sim P^{-2/3}r_p^{3/2}t_{\text{LISA}}$. The last equation indicates that the binary population with longer orbital period contribute less SNR to the GW background. Therefore, neglecting wide WD-MBHs should not qualitatively change the result about the GW background.

Finally, we point out two caveats of this work. First, the GW background derived in this work should be regarded as a lower limit because the calculation is based on the five QPEs detected so far. If more QPEs would be discovered in the future, the GW background would increase as $\sqrt{n_*}$. Second, whether QPEs are made of WDs moving on eccentric orbits around MBHs is still unclear. Further theoretical work is needed to identify observable signatures that can be used to distinguish different models.

ACKNOWLEDGMENTS

This work is supported by the National Science Foundation of China grants No 11991053 and 11873022, and the China Manned Spaced Project (CMS-CSST-2021-B11).

REFERENCES

- Amaro-Seoane, P., Gair, J. R., Freitag, M., et al. 2007, *Classical and Quantum Gravity*, 24, R113, doi: [10.1088/0264-9381/24/17/R01](https://doi.org/10.1088/0264-9381/24/17/R01)
- Amaro-Seoane, P., Audley, H., Babak, S., et al. 2017, arXiv e-prints, arXiv:1702.00786. <https://arxiv.org/abs/1702.00786>
- Arcodia, R., Merloni, A., Nandra, K., et al. 2021, *Nature*, 592, 704, doi: [10.1038/s41586-021-03394-6](https://doi.org/10.1038/s41586-021-03394-6)
- Babak, S., Gair, J., Sesana, A., et al. 2017, *PhRvD*, 95, 103012, doi: [10.1103/PhysRevD.95.103012](https://doi.org/10.1103/PhysRevD.95.103012)
- Barack, L., & Cutler, C. 2004, *PhRvD*, 70, 122002, doi: [10.1103/PhysRevD.70.122002](https://doi.org/10.1103/PhysRevD.70.122002)

- Berry, C., Hughes, S., Sopena, C., et al. 2019, *BAAS*, 51, 42. <https://arxiv.org/abs/1903.03686>
- Bogdanović, T., Cheng, R. M., & Amaro-Seoane, P. 2014, *ApJ*, 788, 99, doi: [10.1088/0004-637X/788/2/99](https://doi.org/10.1088/0004-637X/788/2/99)
- Bonetti, M., & Sesana, A. 2020, *PhRvD*, 102, 103023, doi: [10.1103/PhysRevD.102.103023](https://doi.org/10.1103/PhysRevD.102.103023)
- Chakraborty, J., Kara, E., Masterson, M., et al. 2021, *ApJL*, 921, L40, doi: [10.3847/2041-8213/ac313b](https://doi.org/10.3847/2041-8213/ac313b)
- de Freitas Pacheco, J. A., Filloux, C., & Regimbau, T. 2006, *PhRvD*, 74, 023001, doi: [10.1103/PhysRevD.74.023001](https://doi.org/10.1103/PhysRevD.74.023001)
- Gair, J. R., Babak, S., Sesana, A., et al. 2017, in *Journal of Physics Conference Series*, Vol. 840, *Journal of Physics Conference Series*, 012021, doi: [10.1088/1742-6596/840/1/012021](https://doi.org/10.1088/1742-6596/840/1/012021)
- Gair, J. R., Vallisneri, M., Larson, S. L., & Baker, J. G. 2013, *Living Reviews in Relativity*, 16, 7, doi: [10.12942/lrr-2013-7](https://doi.org/10.12942/lrr-2013-7)
- Giustini, M., Miniutti, G., & Saxton, R. D. 2020, *A&A*, 636, L2, doi: [10.1051/0004-6361/202037610](https://doi.org/10.1051/0004-6361/202037610)
- Han, W.-B., & Fan, X.-L. 2018, *ApJ*, 856, 82, doi: [10.3847/1538-4357/aab03c](https://doi.org/10.3847/1538-4357/aab03c)
- Hils, D., & Bender, P. L. 1995, *ApJL*, 445, L7, doi: [10.1086/187876](https://doi.org/10.1086/187876)
- Ingram, A., Motta, S. E., Aigrain, S., & Karastergiou, A. 2021, *MNRAS*, 503, 1703, doi: [10.1093/mnras/stab609](https://doi.org/10.1093/mnras/stab609)
- Ivanov, P. B. 2002, *MNRAS*, 336, 373, doi: [10.1046/j.1365-8711.2002.05733.x](https://doi.org/10.1046/j.1365-8711.2002.05733.x)
- Ivanov, P. B., & Papaloizou, J. C. B. 2007, *A&A*, 476, 121, doi: [10.1051/0004-6361:20077105](https://doi.org/10.1051/0004-6361:20077105)
- King, A. 2020, *MNRAS*, 493, L120, doi: [10.1093/mnras/slaa020](https://doi.org/10.1093/mnras/slaa020)
- Luminet, J. P., & Pichon, B. 1989, *A&A*, 209, 103
- MacLeod, M., Goldstein, J., Ramirez-Ruiz, E., Guillochon, J., & Samsing, J. 2014, *ApJ*, 794, 9, doi: [10.1088/0004-637X/794/1/9](https://doi.org/10.1088/0004-637X/794/1/9)
- Metzger, B. D., Stone, N. C., & Gilbaum, S. 2021, *arXiv e-prints*, arXiv:2107.13015. <https://arxiv.org/abs/2107.13015>
- Miller, M. C., Freitag, M., Hamilton, D. P., & Lauburg, V. M. 2005, *ApJL*, 631, L117, doi: [10.1086/497335](https://doi.org/10.1086/497335)
- Miniutti, G., Saxton, R. D., Giustini, M., et al. 2019, *Nature*, 573, 381, doi: [10.1038/s41586-019-1556-x](https://doi.org/10.1038/s41586-019-1556-x)
- Motta, S. E., Marelli, M., Pintore, F., et al. 2020, *ApJ*, 898, 174, doi: [10.3847/1538-4357/ab9b81](https://doi.org/10.3847/1538-4357/ab9b81)
- Peters, P. C. 1964, *Physical Review*, 136, 1224, doi: [10.1103/PhysRev.136.B1224](https://doi.org/10.1103/PhysRev.136.B1224)
- Peters, P. C., & Mathews, J. 1963, *Physical Review*, 131, 435, doi: [10.1103/PhysRev.131.435](https://doi.org/10.1103/PhysRev.131.435)
- Raj, A., & Nixon, C. J. 2021, *ApJ*, 909, 82, doi: [10.3847/1538-4357/abdc25](https://doi.org/10.3847/1538-4357/abdc25)
- Reines, A. E., & Volonteri, M. 2015, *ApJ*, 813, 82, doi: [10.1088/0004-637X/813/2/82](https://doi.org/10.1088/0004-637X/813/2/82)
- Robson, T., Cornish, N. J., & Liu, C. 2019, *Classical and Quantum Gravity*, 36, 105011, doi: [10.1088/1361-6382/ab1101](https://doi.org/10.1088/1361-6382/ab1101)
- Rosswog, S., Ramirez-Ruiz, E., & Hix, W. R. 2009, *ApJ*, 695, 404, doi: [10.1088/0004-637X/695/1/404](https://doi.org/10.1088/0004-637X/695/1/404)
- Sesana, A., Vecchio, A., Eracleous, M., & Sigurdsson, S. 2008, *MNRAS*, 391, 718, doi: [10.1111/j.1365-2966.2008.13904.x](https://doi.org/10.1111/j.1365-2966.2008.13904.x)
- Sheng, Z., Wang, T., Ferland, G., et al. 2021, *ApJL*, 920, L25, doi: [10.3847/2041-8213/ac2251](https://doi.org/10.3847/2041-8213/ac2251)
- Shu, X. W., Wang, T. G., Jiang, N., et al. 2017, *ApJ*, 837, 3, doi: [10.3847/1538-4357/aa5eb3](https://doi.org/10.3847/1538-4357/aa5eb3)
- Sigl, G., Schnittman, J., & Buonanno, A. 2007, *PhRvD*, 75, 024034, doi: [10.1103/PhysRevD.75.024034](https://doi.org/10.1103/PhysRevD.75.024034)
- Sigurdsson, S., & Rees, M. J. 1997, *MNRAS*, 284, 318, doi: [10.1093/mnras/284.2.318](https://doi.org/10.1093/mnras/284.2.318)
- Sniegowska, M., Czerny, B., Bon, E., & Bon, N. 2020, *A&A*, 641, A167, doi: [10.1051/0004-6361/202038575](https://doi.org/10.1051/0004-6361/202038575)
- Toscani, M., Rossi, E. M., & Lodato, G. 2020, *MNRAS*, 498, 507, doi: [10.1093/mnras/staa2290](https://doi.org/10.1093/mnras/staa2290)
- Volonteri, M. 2010, *A&A Rv*, 18, 279, doi: [10.1007/s00159-010-0029-x](https://doi.org/10.1007/s00159-010-0029-x)
- Wevers, T., Stone, N. C., van Velzen, S., et al. 2019, *MNRAS*, 487, 4136, doi: [10.1093/mnras/stz1602](https://doi.org/10.1093/mnras/stz1602)
- Xian, J., Zhang, F., Dou, L., He, J., & Shu, X. 2021, *ApJL*, 921, L32, doi: [10.3847/2041-8213/ac31aa](https://doi.org/10.3847/2041-8213/ac31aa)
- Zalamea, I., Menou, K., & Beloborodov, A. M. 2010, *MNRAS*, 409, L25, doi: [10.1111/j.1745-3933.2010.00930.x](https://doi.org/10.1111/j.1745-3933.2010.00930.x)
- Zhao, Z. Y., Wang, Y. Y., Zou, Y. C., Wang, F. Y., & Dai, Z. G. 2021, *arXiv e-prints*, arXiv:2109.03471. <https://arxiv.org/abs/2109.03471>